Int J Adv Manuf Technol (2015) 81:1007–1016
DOI 10.1007/s00170-015-7272-2

ORIGINAL ARTICLE

# Effect of fluid in molten pool on the welds with Ti-6Al-4V during pulsed arc welding

**Mingxuan Yang**[1] **· Zhou Yang**[1] **· Bojin Qi**[1]

Received: 21 January 2015 / Accepted: 4 May 2015 / Published online: 16 May 2015

**Abstract** Titanium alloy is one of the most popular materials in engineering applications. Pulsed arc welding can obtain grain refinement of titanium that is a benefit for mechanical properties. However, the study found that the optimized effect decreased with some higher frequencies. Hence, the study of Ti-6Al-4V was carried out with higher-frequency region, and the reason was discussed. The fluid of molten pool had effect on microstructure and mechanical properties of welding joints. Simultaneously, the arc behavior with pulsing current was known as the important factor for the fluid status. Thus, the microstructural morphology, microhardness gradient, and mechanical properties were detected, which were also compared with other frequencies. With high frequency more than 50 kHz, the fluidity of molten pool decreased significantly with low ductility of joints. The mechanism simulation was produced with plane and ellipsoid assumptions, and the results indicated that the conflux caused impact region of double circulation, which was recognized as the main reason for the drops of microstructure and properties with more than 50 kHz.

**Keywords** Molten pool · Fluid · Ultra high-frequency pulsed arc welding · Mechanical properties

## 1 Introduction

Titanium alloy had super plasticity, high toughness with excellent resistance for corrosion, and fatigue [1]. They have been widely used in the industrial areas, such as aeronautics, astronautics, and transportation engineering [2, 3]. Especially, Ti-6Al-4V titanium alloys were popular in the engineering. As high chemical activity, titanium alloys are easy to suffer from harmful gas and others; hence, gas tungsten arc welding (GTAW) is the preferred method [4]. However, conventional thermal cycle with arc welding caused overheating to the base metal, which is recognized as the reason for the obvious grain growth [5, 6]. Several researchers proved that pulsed welding had a significant impact on the refinement of weld grain [7, 8]. Furthermore, pulsed frequency welding can improve the mechanical properties of welding joints, such as ductility and toughness [9]. Fluid status is the important factor for metallurgical process that is essential to microstructure and joint properties. And, fluid of the molten pool had effect on subsequent heat transfer and solidification of welds [10]. As known, electromagnetic force, surface tension, buoyancy, and plasma force are the main driving forces of fluid of molten pool [11, 12]. Since 1980s, several scholars indicated that fluid in welding pool by electromagnetic force was downward to the deep that caused large penetration [13, 14]. Further study proved that the fluids driven by surface tension and electromagnetic force were opposite, which exist during welding process [15, 16]. The effect on weld geometry was produced with pulsed welding process, and the results indicated a significant positive effect on most of the important bead parameters [17]. Previous results indicated that arc behavior had huge effect on flowing fluid of molten pool [18], especially arc force. Large arc force made surface depression of molten pool that caused forced vortex fluid [19]. As a result, arc force was downward as large driven force for the fluid. With high-

✉ Mingxuan Yang
yangmingxuan@buaa.edu.cn

[1] Department of Materials Processing, Beijing University of Aeronautics and Astronautics, No.37, Xueyuan Road, Beijing 100191, China

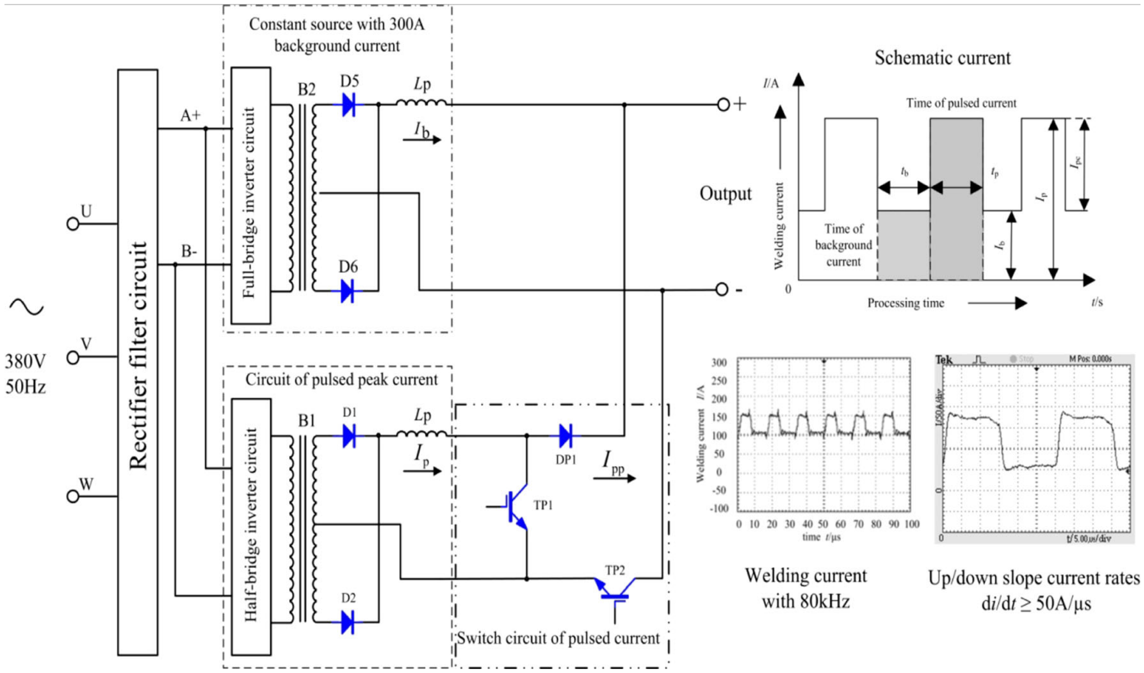

Fig. 1 Welding current with UHFP-GTAW

frequency pulse welding process, the higher frequency, the larger arc force was obtained [20, 21]. Axial arc force could make surface deformation of molten pool, and weld depth was determined by composite vortex intensity.

The previous work [22] mentioned titanium alloys with 0~40 kHz, which indicated that the microstructure and properties were improved with pulsed arc welding. However, the experiments with >40 kHz were not mentioned. On the other side, fluid in molten pool is important for metallurgical process as double circulation. As the arc behavior had huge impact on fluid metal while thermal process, different statuses exist with different pulsed frequencies that caused microstructural characteristics. Hence, the study on effect of fluid in molten pool with ultra high-frequency pulsed gas tungsten arc welding (UHFP-GTAW) was produced. Welding experiment was carried out with Ti-6Al-4V titanium alloy. And, microstructure and joint mechanical properties were discussed with different parameters. The simulation model was established to analyze fluid convections, with which mechanism research supplied proof to experiments.

## 2 Experimental methods

### 2.1 Welding experiments and joint tests

Ti-6Al-4V titanium alloy was picked with the dimensions of 200 mm×80 mm×1.5 mm. As most of research were mentioned with less than 1 kHz, ultra high pulsed frequency of 10~80 kHz was carried out with current upslope/downslope rate (d$i$/d$t$) more than 50 A/μs. The schematic of the weld current is illustrated in Fig. 1a, where $I_b/I_p$ was the background/pulsed current and $f$ the pulse frequency. Time of background and pulsed currents were $t_b$ and $t_p$, respectively,

**Table 1** Parameters of welding process for Ti-6Al-4V titanium alloys

| No. of group | $I_b$/A | $I_p$/A | $f$/kHz | $\delta$ (%) | Argon $q_c$/(L min$^{-1}$) | | | Welding speed $v$/(mm min$^{-1}$) |
|---|---|---|---|---|---|---|---|---|
| | | | | | Torch | Welds back | Trailer | |
| 1 | 90 | - | - | - | 15 | 20 | 3 | 200 |
| 2 | 45 | 115 | 10 | 50 | 15 | 20 | 3 | 200 |
| 3 | 45 | 115 | 20 | 50 | 15 | 20 | 3 | 200 |
| 4 | 45 | 115 | 30 | 50 | 15 | 20 | 3 | 200 |
| 5 | 45 | 115 | 40 | 50 | 15 | 20 | 3 | 200 |
| 6 | 45 | 110 | 50 | 50 | 15 | 20 | 3 | 200 |
| 7 | 55 | 100 | 80 | 50 | 15 | 20 | 3 | 200 |

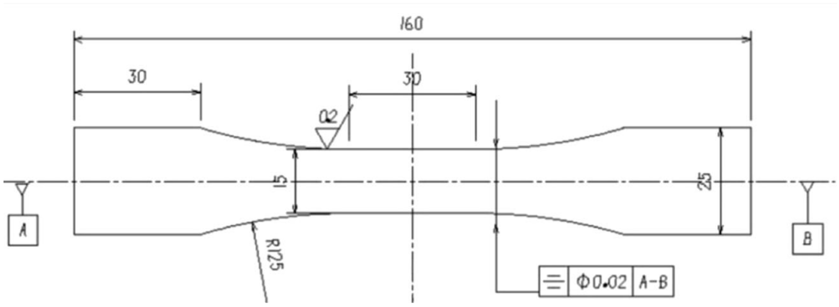

**Fig. 2** Specimen dimensions for fatigue property tests

and duty cycle of pulse duration can be deduced as $\delta=t_p/(t_b+t_p)$. The waveform of arc voltage and welding current is shown in Fig. 1b.

All of the welding experiments were processed with similar condition of constant penetration. The welds were one-side welding with backing during both conventional and pulsed welding methods. The parameters are shown in Table 1. As large penetration of welds by UHFP-GTAW that has been approved from previous work, average welding current was chosen a little less with more than 50 kHz. The 160-mm length welds were obtained along the welding direction without a wire. The conventional parameters were as follows: the electrode radius was 1.2 mm and made of 2 % cerium and 98 % tungsten; the arc length was 3 mm; the gas was 99.99 % argon. Etch solution of $HF/HNO_3/H_2O=1:6:13$ (volume) was used to remove the oxide film of workpiece. Then, the workpieces were preserved in a dry-cleaning utensil until welding, and the conserved time was less than 24 h.

Metallographic specimens were etched by a solution with a volume ratio of $HF/HNO_3/H_2O=3:10:100$. The microstructure was captured with OLYPUMS BX51M. A digital Vickers hardness tester (DHV-1000) was used to measure microhardness, and 4.9 N load was carried out with 15-s loading time for every test point and a constant distance of 0.2 mm between every two locations. Three specimens were prepared for each parameter with mechanical property tests. The tensile tests were completed with strain rate of $9\times10^{-4}$ $s^{-1}$ (DWD-50E). The grain size was captured with intercept method. The methods and specimen above have been described in previous work [22]. SCHENCK 64kN was picked up for low cycle fatigue test (10 Hz) with 600-MPa constant load that is displayed in Fig. 2.

## 2.2 Simulation procedure

Fluid in molten pool was supposed to be the important factor for microstructural morphology. Thus, the simulation was carried out for supporting the mechanism study. Physical properties of Ti-6Al-4V are listed in Table 2. Titanium alloys are paramagnetic materials; as a result, the magnetic permeability $\mu_m$ was substituted by $\mu_0$. The heat fluxes on the other boundaries were zero, and welding heat input was at the surface depression. Figure 3 indicates that 2D model with ellipsoid surface depression was produced for transient status under the effect of arc force. The followed assumptions were as follows:

a. The liquid in molten pool could be recognized as viscous, incompressible, laminar fluid;
b. Density variations follow the *Boussinesq* approximation;

**Table 2** Physical properties of Ti-6Al-4V

| Physical properties | Value |
|---|---|
| Liquidus temperature $T_l$(K) | 1928 [25] |
| Solidus temperature $T_s$(K) | 1878 |
| Liquid density $\rho$(kg/m$^3$) | 4300 |
| Liquid viscosity $\mu$(kg/ms) | 0.0049 |
| Solid phase effective thermal conductivity $k_s$(J/ms·K) | 5.4 |
| Liquid phase effective thermal conductivity $k_l$(J/ms·K) | 15.9 |
| Solid phase specific heat capacity $C_{PS}$(J/kg·K) | 879 |
| Liquid phase specific heat capacity $C_{PS}$(J/kg·K) | 678 |
| Temperature coefficient of surface tension d$\gamma$ /d$T$(N/mK) | −0.00028 |
| Thermal expansion coefficient $\beta$(K$^{-1}$) | $1.1\times10^{-5}$ [26] |
| Magnetic permeability of vacuum $\mu_0$(N/A$^2$) | $1.26\times10^{-6}$ |
| Melting heat $L$(J/kg) | $3.57\times10^5$ |
| Surface tension $\sigma$(mN/m) | 1650 |

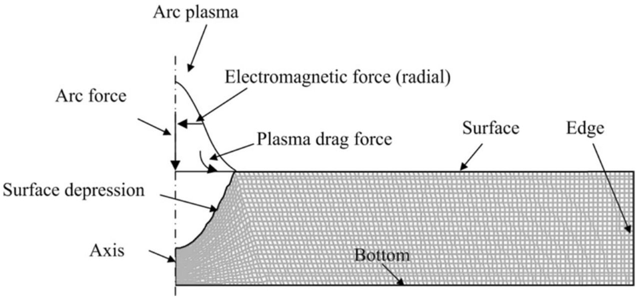

**Fig. 3** 2D model with surface depression for simulation

c. The physics of material are independent of temperature except for surface tension coefficient.

The heat input followed Gauss distribution that was represented in Eq. 1.

$$Q = 3\cdot\eta\cdot\frac{UI}{\pi\cdot R_{\mathrm{arc}}^2}\exp\left(-\frac{3r_0^2}{R_{\mathrm{arc}}^2}\right) \tag{1}$$

Where,

| | |
|---|---|
| $Q$ | heat input |
| $\eta$ | efficiency |
| $U$ | arc voltage (average value) |
| $I$ | welding current (average value) |
| $R_{\mathrm{arc}}$ | radius of arc plasma |
| $r_0$ | radius of random position under arc plasma. |

The model follows mass conservation equation, momentum conservation equation of x/y direction, and energy conservation equation, which were represented in Eqs. 2~4. Driving forces, such as surface tension, electromagnetic force (Eq. 5), and buoyancy, were known as the source term by momentum equation of x/y direction. That meant the source terms in Eq. 3, $S_x$ and $S_y$ equaled zero. There were no mass exchange and internal/external energy source mentioned in the simulation. As a result, the source terms in Eq. 2, 4 also equaled zero, respectively.

For C-GTAW, plane assumption has been carried out as the surface depression caused by arc force can be ignored. By contrast, 2D model with 80 kHz followed Fig. 3. Notice that the previous work on surface depression has analyzed the effect of arc force on molten pool. The arc force at 80 kHz was much larger than others. And, ellipsoid surface depression can be used with such condition. During the analysis in this paper, the results with 80 kHz would be compared with C-GTAW. The melting status and fluid velocity would be mentioned as the important factors, which were used to evaluate the fluidity of molten pool.

$$\frac{\partial\rho}{\partial t} + \nabla\cdot(\rho V) = S_m \tag{2}$$

$$\begin{cases} \dfrac{\partial(\rho V_x)}{\partial t} + \nabla\cdot(\rho\mathbf{V}V_x) = \mu\nabla^2 V_x - \dfrac{\partial P}{\partial x} + S_x \\ \dfrac{\partial(\rho V_y)}{\partial t} + \nabla\cdot(\rho\mathbf{V}V_y) = \mu\nabla^2 V_y - \dfrac{\partial P}{\partial y} + S_y \end{cases} \tag{3}$$

$$\frac{\partial(\rho h)}{\partial t} + \nabla\cdot(\rho\mathbf{V}h) = k\nabla^2 h + S_y \tag{4}$$

$$\begin{cases} (J\times B)_x = \dfrac{-\mu_0 I^2}{4\pi^2 R_{\mathrm{arc}}^2 r}\exp\left(\dfrac{-r^2}{2R_{\mathrm{arc}}^2}\right)\left[1-\exp\left(\left(\dfrac{-r^2}{2R_{\mathrm{arc}}^2}\right)\right)\right]\left(1-\dfrac{x}{h}\right) \\ (J\times B)_y = \dfrac{-\mu_0 I^2}{4\pi^2 h r^2}\left[1-\exp\left(\left(\dfrac{-r^2}{2R_{\mathrm{arc}}^2}\right)\right)\right]^2\left(1-\dfrac{y}{h}\right) \end{cases} \tag{5}$$

Where,

| | |
|---|---|
| $R_{\mathrm{arc}}$ | groove radius of arc plasma |
| $h$ | arc length |
| $x$ | x coordinate |
| $y$ | y coordinate. |

The arc force distribution was added at the axis as the plane assumption was picked with C-GTAW. However, the effect area was less than 0.2-mm depth because the arc force was too little. With UHFP-GTAW, the surface depression occurred with melting status; thus, the initial temperature was 1800 K that was nearly the solidus temperature.

## 3 Results and discussion

### 3.1 Microstructure of the as-weld condition

After the thermal cycle of GTAW process, grain growth of Ti–6Al–4V was significant compared with base metal as shown in Fig. 4. The average grain size increased from 5 μm to about

**Fig. 4** Grain growth with GTAW thermal process

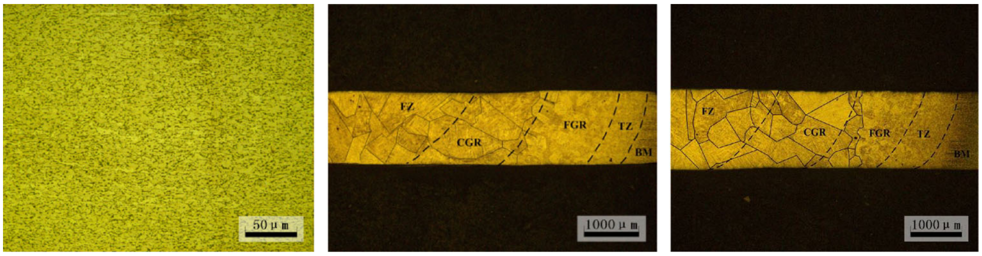

(a)Base metal (b) Conventional GTAW (c) $f$=80 kHz

**Fig. 5** Microstructure with 80 kHz (×200)

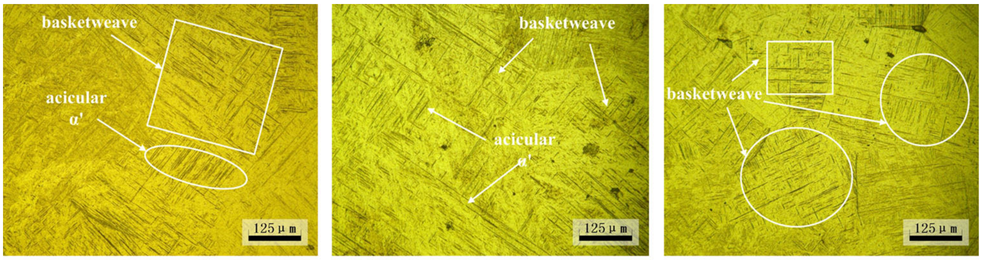

(a) Fusion zone (b) Coarse-grain region (c) Fine-grain region

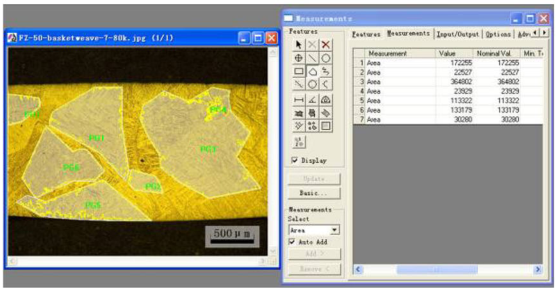

| | Measurement | Value | Nominal Val. | Min. T |
|---|---|---|---|---|
| 1 | Area | 172255 | 172255 | |
| 2 | Area | 22527 | 22527 | |
| 3 | Area | 364802 | 364802 | |
| 4 | Area | 23929 | 23929 | |
| 5 | Area | 113322 | 113322 | |
| 6 | Area | 133179 | 133179 | |
| 7 | Area | 30280 | 30280 | |

(d) distribution density of basketweave

170 μm. The macrostructure of the welds is divided into the following regions: fusion zone (FZ), coarse-grained region (CGR), fine-grained region (FGR), transition zone (TZ), and base metal (BM).

With higher pulsed frequencies 80 kHz, the average grain size was 164 μm in the FZ that was a little bigger than others during 20~40 kHz. Figure 5a–c shows the microstructure with different regions of 80 kHz. The basketweave and acicular α' can be found in the FZ, and the distribution density was still large with more than 60 % that can be calculated by area measurement with the metallographic photo (Fig. 5d). However, the microstructural morphology in CGR was much more different than that with previous frequencies. The distribution of basketweave decreased, and long acicular α′ paralleled, among which short needle existed. In contrast with 30-kHz pulsed frequency [22], the amount of long acicular morphology decreased significantly. Furthermore, the basketweave in the CGR (Fig. 5b) was difficult to distinguish. The basketweave was believed to have effect on preventing the crack propagation. As a result, the microstructural morphology mentioned above caused low resistance for cracking in CGR with 80 kHz. Figure 5c illustrates the FGR, and the

**Fig. 6** Microstructure with 50 kHz

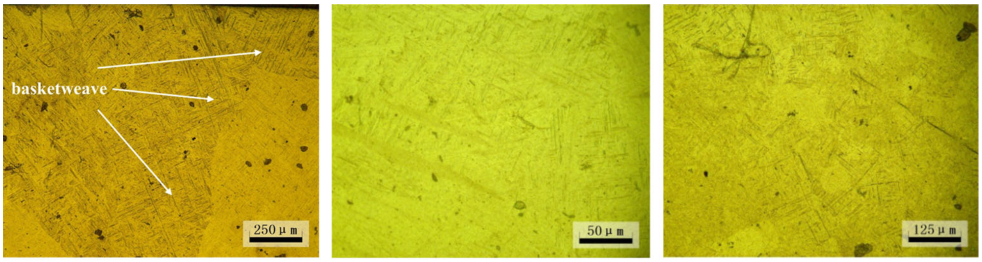

(a) Fusion zone(×100) (b) Coarse-grain region(×500) (c) Fine-grain region(×200)

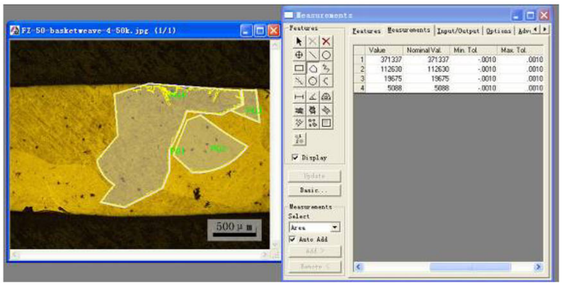

| | Value | Nominal Val. | Min. Tol. | Max. Tol. |
|---|---|---|---|---|
| 1 | 371337 | 371337 | -.0010 | .0010 |
| 2 | 112630 | 112630 | -.0010 | .0010 |
| 3 | 19675 | 19675 | -.0010 | .0010 |
| 4 | 5088 | 5088 | -.0010 | .0010 |

(d) distribution density of basketweave

result indicated the basketweave and short acicular $\alpha'$ distributed in the field of view, which also meant that this region also owned high resistance to crack. The fracture can be predicted to happen near the CGR with 80 kHz.

With 50 kHz, the grain size was 12 % bigger than other frequencies; however, it still decreases by 14.8 % compared with C-GTAW. Figure 6 illustrates few basketweave or acicular $\alpha'$ distributed, although such basketweave can be found in FZ with considerable distributing density. Even in FGR, it was hard to verify obvious basketweave compared with other frequencies, which meant that the backward or drop of microstructure happened with 50 kHz. Furthermore, it is known that the basketweave can decrease the possibility of crack propagation due to microstructure-induced crack deflection, branching, and closure [23]. Hence, it can be predicted that the joints' properties would change at some frequencies, which inferred the low cracking resistance happened. As described before, the effect of arc behavior on fluid metal was enhanced, which would have impact on microstructures. As a result, it was necessary to check whether the properties changed in the region of more than 50 kHz.

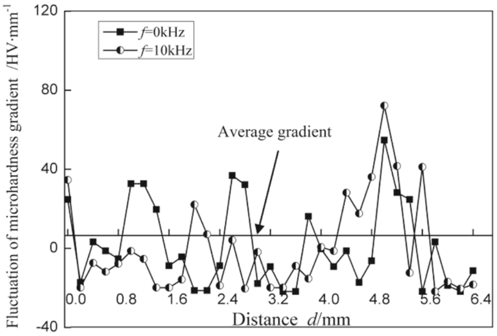

(a) C-GTAW & $f$=10kHz

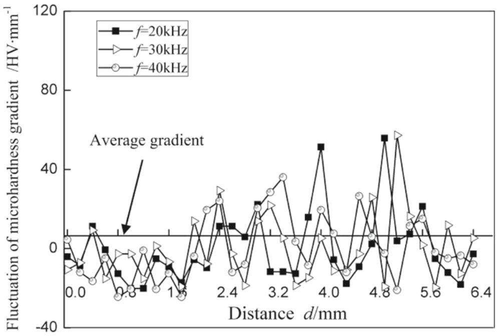

(b) 20~40 kHz

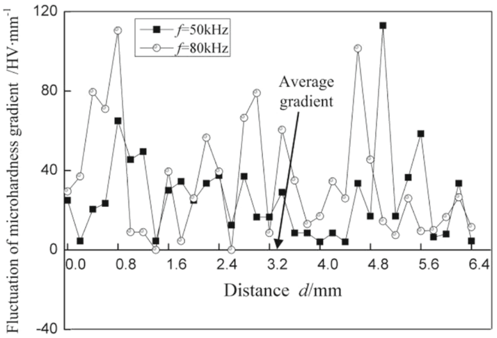

(c) 50kHz & 80kHz

**Fig. 7** Fluctuation of microhardness gradient

**Table 3** Tensile properties

| No. | Elongation $A$/% | Percentage of reduction of area $Z$/% |
|---|---|---|
| 1 | 3.7 | 5.7 |
| 2 | 5.8 | 9.1 |
| 3 | 4.9 | 16.1 |
| 4 | 6.2 | 14.2 |
| 5 | 5.1 | 16.2 |
| 6 | 5.7 | 8.5 |
| 7 | 6.2 | 7.4 |

### 3.2 Microhardness gradient

Microhardness gradient was supposed to check microhardness gap between the measured positions nearby, which showed how much different between them. Here, the paper defined variable $F$ to evaluate fluctuation of microhardness gradient by Eq. 4. Big fluctuation ($F$) indicated that the large differences existed, and small fluctuation ($F$) pointed out the corresponding little difference, which can be recognized as the degree of similarity of the weld microstructure. Thus, the paper used the variable $F$ to evaluate the uniformity of microstructure.

$$F = Gradient(\mathrm{i}) - Gradient(\mathrm{avg}) \tag{6}$$

Where,

| | |
|---|---|
| $Gradient$(i) | microhardness gradient of certain parameter |
| $Gradient$(avg) | average microhardness gradient of certain frequency. |

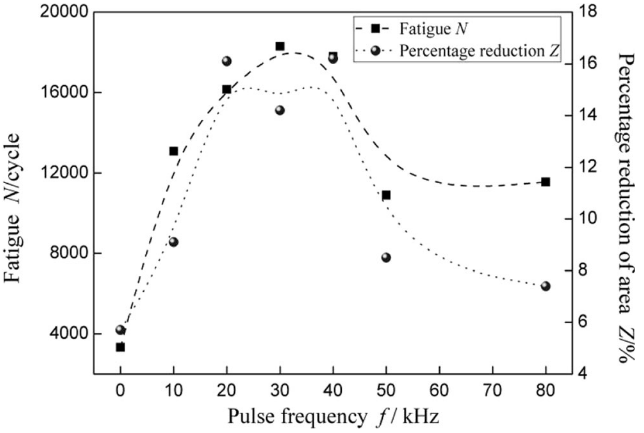

**Fig. 8** Fatigue test of welding joints

**Fig. 9** Molten pool

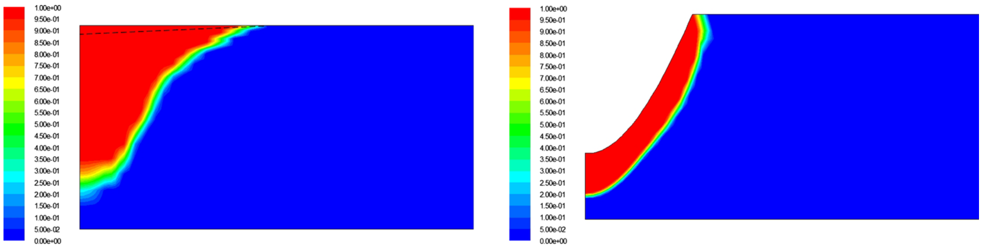

(a) molten with C-GTAW (b) molten with *f* =80 kHz

Variable *F* is illustrated in Fig. 7. The average gradient was calculated to be the datum. The fluctuation was obvious between C-GTAW and 10 kHz. But, all the data distributed around the average gradient. It can be found that fluctuation of microhardness gradient was smaller with 20~40 kHz than other frequencies. Most of the data distributed around the average gradient. However, when the frequency was more than 50 kHz, *F* fluctuated significantly, and most data derivate from the average gradient. The measured results coincided with the changing of the microstructural morphology in Sect. 3.1. And, more mechanical property tests were necessary to check the effect of such frequencies and also the mechanism of metallurgical process.

## 3.3 Mechanical properties

### *3.3.1 Tensile test*

Table 3 shows the tensile properties of specimens. The tensile strength maintained a relatively stable state with both conventional and UHFP-GTAW process, which was approximately equal to that in the BM. That demonstrated that the impact of double circulation had little effect on tensile strength. During the further study for ductility of joints, the results by C-GTAW were regarded as the standard while analyzing. Elongation, *A*, and reduction of area, *Z*, were measured for ductility of welding joints. Compared with C-GTAW, the elongation increased by 32~68 % with 10–80 kHz. Meanwhile, the reduction of area *Z* increased with larger frequency below 40 kHz, and by more than 180 % at most. The heat input of each parameter was calculated. The results showed that with the same welding current, 30 and 40 kHz can obtain one-double side welds with lower arc voltage, which created less heat input than C-GTAW. The uniform basketweave and short acicular $\alpha'$ martensite distributed in the FZ, which can decrease the possibility of crack propagation. However, the increased ratio decreased when pulse frequency was more than 50 kHz again, which declared the reduction of area dropped during high frequencies. The distribution of basketweave that decreased in the CGR (Figs. 5b and 6b) can be recognized as the reason.

### *3.3.2 Fatigue life test*

Fatigue life test was carried out for evaluating ductility of welding joints by cycle *N*. And, the results are illustrated in Fig. 8. Compared with C-GTAW, it was improved absolutely with UHFP-GTAW, especially at 30~40 kHz. In that region of pulse frequency, the fatigue lives were 18,287 and 17,791, respectively, which were four times larger than that with C-GTAW. However, it decreased when frequency was more than 50 kHz either, which displayed similar trend with reduction of area.

Above all, the microstructural morphology and joint properties were beyond the trend with high frequencies. In that region, the basketweave and short acicular $\alpha'$ were undistinguished in CGR which was known as the hazardous area of fracture. The microhardness gradient fluctuated significantly that inferred the reduction of microstrutural uniformity. Furthermore, the joints' ductility dropped down with decreasing fatigue strength, which demonstrated the low cracking resistance. The experiments and tests produced the weak area of pulsed arc welding process with microstructures and properties. Hence, the mechanism study was carried out below with fluid in molten pool.

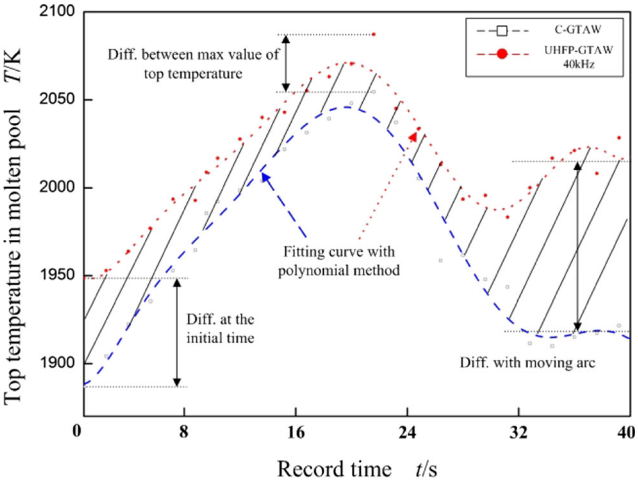

**Fig. 10** Thermal observation for the top temperature in molten pool

**Fig. 11** Fluid velocity in molten pool (colored by velocity)

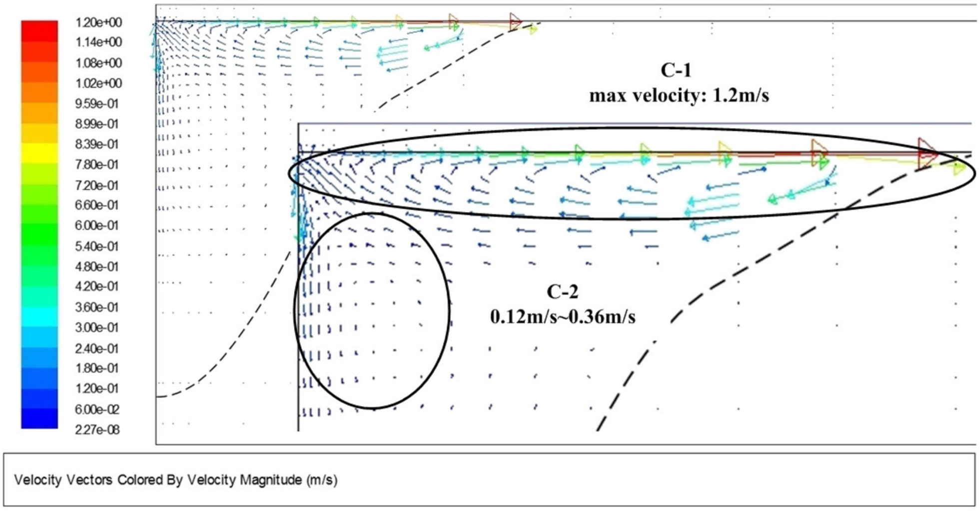

(a) C-GTAW

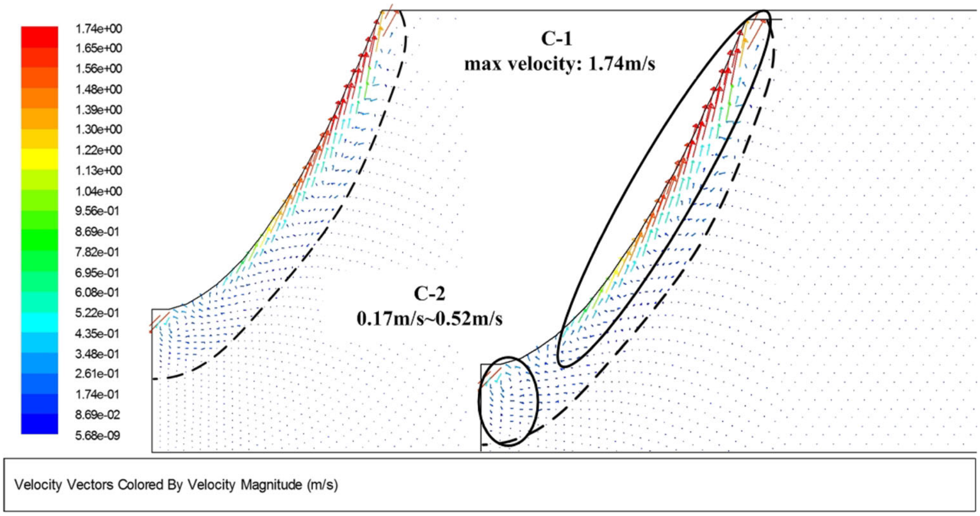

(b) *f* =80 kHz

### 3.4 Fluid of molten pool

The simulated molten pool and temperature distributions were displayed with different welding methods, which are illustrated in Fig. 9a, b. Simulated work with 80 kHz has been discussed in reference [24]. The results would be discussed with the C-GTAW in this section. As little surface depression with C-GTAW, plane assumption was used with the error less than 2 %. Large depression was caused by the arc force with UHFP-GTAW in Fig. 9b, and ellipsoid assumption was carried out with error also less than 2 %.

With thermal observation, the temperature of 40 kHz increased 35~120 K at 60 A average current level. The fitting curves are illustrated in Fig. 10. The gap between C-GTAW and 40 kHz was more than 60 K at welding start time. Then, the top temperature increased to the max value and the gap reduced. When the arc began to move, both of the top temperature decreased. Finally, it came to be stable with moving arc. Notice that the results with 80 A cannot be captured subjected

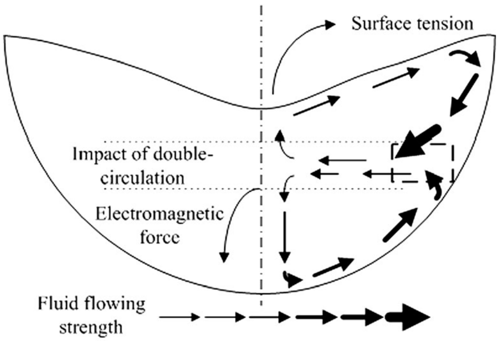

**Fig. 12** Conflux of two circulations

to the accuracy of the imager and filter lens. With 80 kHz at 80 A, the paper predicted that there was the larger temperature gap than 60 A. As known, the temperature distribution was the key for surface tension gradient and viscosity, which affected fluidity of molten pool. The large temperature gradient can create large velocity of Marangoni convection and decreasing viscosity, which was important for the fluidity. Such distribution revealed large energy density of heat input with 40 kHz that was a benefit for metallurgical process and microstructure growth. However, too large fluid velocity may cause weakness of molten pool that would be discussed below.

The fluid statuses with C-&UHFP-GTAW are illustrated in Fig. 11. C-1, Marangoni convection, was driven by surface tension distributing around surface of pool, and C-2 by electromagnetic force (Fig. 11a) was the fluid with C-GTAW. The results indicated that double circulation fluid can be ignored as the little arc force. Except for the interface of liquid and arc plasma, little velocity existed with less than 0.12 m/s. The maximum value happened in the region of the arc force that was up to nearly 0.36 m/s. And, the larger arc force had been the main factor for the surface depression of molten pool with 80 kHz. The velocity of C-2 was 0.17~0.52 m/s with the average more than 0.4 m/s. And, the maximum value also happened in the region of the arc force that was 1.5 m/s.

In Fig. 11, the velocity of Marangoni convection was 1.2 m/s with C-GTAW. In contrast, with 80 kHz, it was 1.74 m/s during UHFP-GTAW that increased by 45 % than former. On the other side, the velocity of C-2 increased by more than 300 %. Thus, the fluidity of molten pool was improved significantly with UHFP-GTAW according to the simulation results.

Furthermore, the average velocity of C-2 was less than 0.12 m/s with C-GTAW. It was just 10 % of C-1 (1.2 m/s) by surface tension, and it could be ignored in some case. With 80 kHz, the velocity increased by 3 times as the effect of larger arc force, and the average velocity was more than 0.4 m/s. During UHFP-GTAW, the velocity of C-1 increased to 1.74 m/s, compared to which the velocity of C-2 was 25 % of it. That meant that the velocity of C-2 took more portion of C-1 with high pulsed frequency.

In the molten pool, Fig. 12 displays the conflux mentioned above, where two circulations crashed together. With less velocity of C-2, the effect of crashing between two circulations can be ignored. However, the velocity of the two circulations increased with more than 50 kHz significantly. That will enhance the strength of the crash. While the surface depressed with large arc force, the impact of C-2 to C-1 became significant. The conflux obtained little fluidity although both circulations 1 and 2 had larger velocity. The transferred heat flux would slow down with liquid metal. As a result, the microstructural uniformity and temperature distribution would be influenced. That can be recognized as the reason for the drops of microstructure and joint properties with more than 50 kHz.

## 4 Conclusions

The drops of microstructure and joint properties were found with experiments that indicated the backward exist during some higher frequencies; however, it was also much better than that with C-GTAW. The results supplied evidence with metallographic study, microhardness, and mechanical tests. With high frequency more than 50 kHz, the basketweave and short acicular $\alpha'$ were undistinguished in coarse-grain region where fracture happened frequently, which indicated the lack of cracking resistance. The microhardness gradient fluctuated more obviously, which inferred low microstrutural uniformity. And also, reduction of area and fatigue decreased that revealed worse ductility of joint. The mechanism study was carried out, and the simulation was produced with arc behavior. As lager fluid velocity driven by electromagnetic force, double circulation can be found during pulsed arc welding of Ti-6Al-4V, and the fluidity of molten pool decreased because of the crashing region, fluid conflux. The conflux region of double circulation was at middle of the weld cross section. And, the impact of two circulations was considered as the reason for changing of microstructural morphology with higher frequencies of 50~80 kHz.

**Acknowledgments** This work was supported by the National Natural Science Foundation of China under grant No. 51405007 and Fundamental Research Funds for the Central Universities. The authors acknowledge Beijing University of Aeronautics and Astronautics for supporting our research. All forms of support are greatly appreciated.

## References

1. Leyens C, Peters M (2003) Titanium and titanium alloys. Wiley-VCH Verlag GmbH & Co. KGaA, Weinheim
2. Malinov S, Sha W (2004) Application of artificial neural networks for modeling correlations in titanium alloy [J]. Mater Sci Eng A 365(1):202–211
3. Balasubramanian M, Jayabalan V, Balasubramanian V (2008) A mathematical model to predict impact toughness of pulsed-current gas tungsten arc-welded titanium alloy [J]. Int J Adv Manuf Technol 35(9–10):852–858
4. Balasubramanian M, Jayabalan V, Balasubramanian V (2009) Effect of pulsed gas tungsten arc welding on corrosion behavior of Ti-6Al-4V titanium alloy [J]. Mater Des 29(7):1359–1363
5. Qi Yunlian J, Deng QH, Zeng L (2000) Electron beam welding, laser beam welding and gas tungsten arc welding of titanium sheet [J]. Mater Sci Eng A 280(1):177–181
6. Baeslack WA III, Banas CM (1981) A comparative evalution of laser and gas tungsten arc weldments in high temperature titanium alloys [J]. Weld J 60(7):121–130
7. Ge ZX, Chen HM, Ge Y (2004) Affection of arc-weld inversion power's frequency on weld grain's thinning [J]. Hot Work Technol 7:47–48
8. Balasubramanian V, Jayabalan V, Balasubramanian M (2008) Effect of current pulsing on tensile properties of titanium alloy [J]. Mater Des 29(7):1459–1466

9. Balasubramanian M, Jayabalan V, Balasubramanian V (2008) Effect of microstructure on impact toughness of pulsed current GTA-welded $\alpha+\beta$ titanium alloy [J]. Mater Lett 62(6):1102–1106
10. Jamshidi Aval H, Farzadi A, Serajzadeh S, Kokabi AH (2009) Theoretical and experimental study of microstructures and weld pool geometry during GTAW of 304 stainless steel [J]. Int J Adv Manuf Technol 42(11–12):1043–1051
11. Kim WH, Fan HG, Na SJ (1997) Effect of various driving forces on heat and mass transfer in arc welding [J]. Numer Heat Tr A-Appl 32(6):633–652
12. Oreper GM, Szekely J (1987) A comprehensive representation of transient weld pool development in spot welding operations [J]. Metall Trans A 18(7):1325–1332
13. Kou S, Wang YH (1986) Computer simulation of convection in moving arc weld pools [J]. Metall Trans A 17(12):2271–2277
14. Tsai MC, Kou S (1990) Electromagnetic force induced convection in weld pool with a free surface [J]. Weld J 69(6):241–246
15. Kou S, Wang YH (1986) Weld pool convention and its effect [J]. Weld J 65(3):63–70
16. Fan HG, Tsai HL, Na SJ (2000) Heat transfer and fluid flow in a partially or fully penetrated weld pool in gas tungsten arc welding [J]. Int J Heat Mass Transf 44(2):417–428
17. Balasubramanian M, Jayabalan V, Balasubramanian V (2010) Effect of process parameters of pulsed current tungsten inert gas welding on weld pool geometry of titanium welds [J]. Acta Metall Sin 23(4):312–320
18. Qi BJ, Yang MX et al (2013) The effect of arc behavior on weld geometry by high frequency pulse GTAW process with 0Cr18Ni9Ti stainless steel [J]. Int J Adv Manuf Technol 66:1545–1553
19. Lin ML, Eagar TW (1985) Influence of arc pressure on weld pool geometry [J]. Weld J 64(6):162–169
20. Ghosh PK, Dorn L, Hübner M, Goyal VK (2007) Arc characteristics and behavior of metal transfer in pulsed current GMA welding of aluminum alloy [J]. J Mater Process Technol 194:163–175
21. Onuki J, Anazawa Y, Nihei M, Katou M, Akira O, Takao F (2002) Development of a new high-frequency, high-peak current power source for high constricted arc formation [J]. Jpn J Appl Phys 41(9):5821–5826
22. Mingxuan Y, Bojin Q et al (2013) Effect of pulse frequency on microstructure and properties of Ti-6Al-4V by ultrahigh frequency pulse gas tungsten arc welding [J]. Int J Adv Manuf Technol 68(1–4):19–31
23. Zuo JH, Wang ZG, Han EH (2008) Effect of microstructure on ultra-high cycle fatigue behavior of Ti–6Al–4V [J]. Mater Sci Eng A 473(1):147–152
24. Yang M, Yang Z, Qi B, Cong B (2014) Study on surface depression of molten pool with pulsed welding [J]. Weld J 93(8):312s–319s
25. Boyer R, Welsch G, Collings EW (eds) (1994) Materials properties handbook: Titanium alloys. ASM International, Materials Park (OH)
26. Mishra S, Debroy T (2004) Measurements and Monte Carlo simulation of grain growth in the heat-affected zone of Ti-6Al-4V welds [J]. Acta Mater 52(5):1183–1192